TRANSACTIONS OF THE INSTITUTE OF FLUID-FLOW MACHINERY

No. 121, 2008, 67-84

ADAM PAPIERSKI[1] and GRZEGORZ PECZKIS[2*]

Flow through an eccentric longitudinal clearance ring

[1]*Lodz University of Technology, Institute of Turbomachinery, Wólczańska 219/223, 90-924 Łódź, Poland*
[2]*Silesian University of Technology, Institute of Power Engineering and Turbomachinery, Konarskiego 18, 44-100 Gliwice, Poland*

Abstract

In this work there are presented flow calculation models through the longitudinal eccentric throttle clearance ring. There are shown some calculations for laminar and turbulent flow. Turbulent flow is described as self-similar and with application of model $k-\varepsilon$, the description is illustrated with calculative example. The measurement results of pressure fields measured in the longitudinal eccentric clearance are presented. The calculation results obtained with different methods are compared with one another.

Keywords: Centrifugal pump, Eccentric clearances

Nomenclature

$U_j(j, i = 1, 2, 3)$	–	components of the flow rate vector in a rectangular coordinate system (in T-F), m/s
b, b_m, Δb	–	width of the clearance, mean value of this width, increase in width of the clearance, m
e	–	eccentricity, m
l	–	axial length, m
F_x, F_y, F	–	force (radial force), N
$\Delta p_{1-2}, \Delta p_{wl}, \Delta p_{sz}, \Delta p_{wyl}$	–	total, inlet, continuous, outlet pressure drop in the axial clearance, Pa
p_1, p_2	–	pressure between inlet, outlet in the clearance, Pa
R, r, R_t, R_w	–	radius, radius of sleeve, radius of shaft, m

*Corresponding author. E-mail address: peczkis@wp.pl

Re, Re_P, Re_C	–	Reynolds number, Re_P in Poiseuille's flow, Re_C in Couette's flow,
r, ϕ, z	–	coordinates of the cylindrical coordinate system, m, rad, m
t	–	temperature, $^\circ C$
q	–	flow rate through the clearance, m^3/s
$u = \omega r$	–	circumferential speed of the wall, m/s
v_r, v_ϕ, v_z	–	components of the vector of the flow rate in a cylindrical coordinate system, m/s
x, y, z	–	coordinates of a Cartesian coordinate system, m

Greek symbols

ω	–	angular velocity of the rotating ring, s^{-1}
$\vec{\omega}$	–	angular velocity of the rotating system (in T-F), s^{-1}
φ	–	circumferential coordinate, rad
λ	–	coefficient of the continuity resistance
ρ	–	density of the liquid, kg/m^3
ζ_{wl}	–	coefficient part of the inlet losses
ζ_{wyl}	–	coefficient part of the outlet increase,
$\varepsilon = \frac{e}{b}$	–	relative eccentricity
ε	–	value of the energy of dissipation (in T-F), $\mathrm{m}^2/\mathrm{s}^2$
δ	–	angle of inclination axle
φ_F	–	angle of radial force
μ	–	dynamic viscosity, kg/ms
μ_T	–	dynamic turbulent viscosity (in T-F), kg/m s
$\nu = \mu\rho$	–	kinematic viscosity, m^2/s

1 Introduction

The longitudinal clearance is a crucial element of flow systems in hydraulic machines. In the figure 1, there are shown longitudinal clearances of the centrifugal pumps, which choke the flow by means of: a) impeller neck of single-stage pump, b) stage wheel, c) balance disk set for axial force of multi-stage pump. The sealing

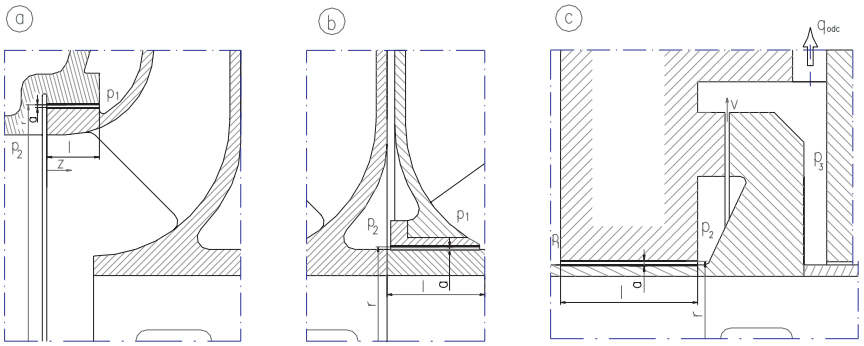

Figure 1. Longitudinal clearances of centrifugal pumps: a) impeller neck, b) stage wheel, c) balance disk set for axial force.

clearance task is to reduce the flow q between spaces with different pressures [19]. The calculations are conducted for laminar and self-similar flow in the computer program written in Fortran language, whereas for three-dimensional turbulent flow in the TascFlow program. The obtained results are subject to further calculative and graphic treatment in the commonly used editor programs.

Time needed for preparation of conduced calculations depends on the level of mastering and knowing the programs. The presented selected measurement results for pressure fields and flow parameters through the longitudinal clearance come from the work [15], where they are described in a greater amount of detail.

2 Theoretical rudiments for modelling the flow through clearances

The geometry of real longitudinal clearances has some characteristic shape errors (Fig. 2):

- eccentricity e,
- non-parallelism of the walls determined with the angle ϑ,
- confusority or diffuseness,

and as a result variable speed, which differs from the rated one (average one) by Δb.

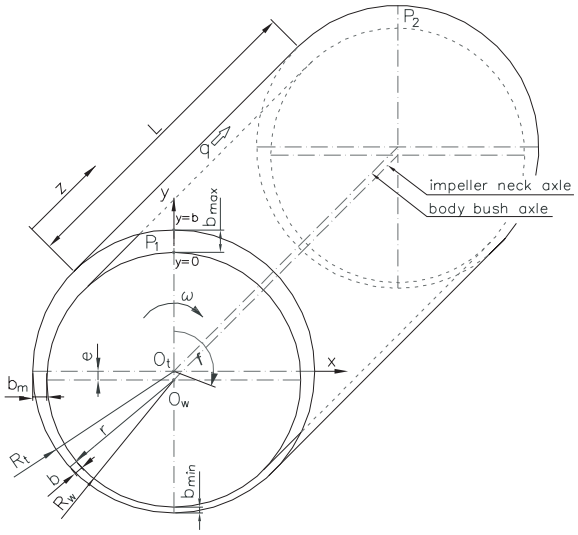

Figure 2. Eccentric longitudinal clearance.

After some time of usage, the erosion can lead to further shape change of the clearances. The width of the clearance b affects the flow stream substantially and as a result the efficiency of hydraulic machine. Widening of the width b, e.g. due to the erosion causes the volumetric efficiency of the machine lower and provides the economic reason for its repair [19].

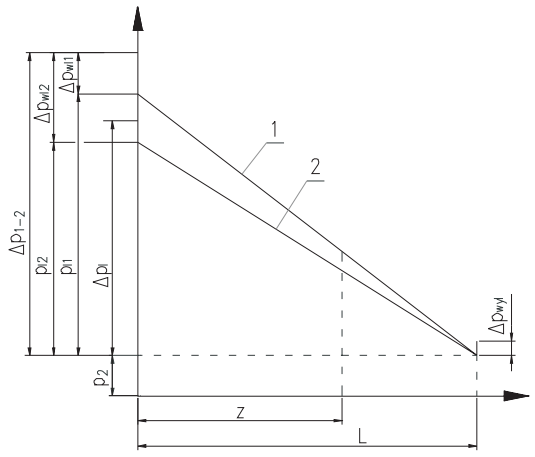

Figure 3. Pressure course in the eccentric clearance for (1) $\varphi = \pi$ is $b = b_m - e$ and for (2) $\varphi = 0$ is $b = b_m + e$.

The eccentricity e is caused by the shaft deflection and the performance inaccuracy of machine components compounding the dimensional chain, which determines the machine. Pressure field asymmetry in the clearance (Fig. 3), caused by the eccentricity and the resultant radial force arising from it, affects the machine dynamic properties significantly, and particularly the shaft deflection and critical rotational speed of the impeller unit [11-13, 5]. Moreover, the eccentricity influences also the leakage q. The angle of wall non-parallelism ϑ affects both the pressure field in the clearance and the flow stream. The present article deals with the eccentric clearance (Fig. 2).

It is practically assumed, that the entire kinetic energy behind the clearance is the subject to dispersion and then the complete pressure drop in the clearance is the sum of [7, 3, 9, 18]:

$$\Delta p = \Delta p_{wl}(\varphi) + \Delta p_{1-2}(\varphi) - \Delta p_{wyl}\,(\varphi)\,. \tag{1}$$

2.1 Part of inlet pressure drop

Flow at the inlet causing local pressure loss has turbulent character, regardless of the flow character in the clearance alone. At the inlet to the clearance, the

pressure drop is:

$$\Delta p_{wl}(\varphi) = \rho\left(\zeta_{wl}\right)\frac{w^2}{2}, \tag{2a}$$

$$\Delta p_{1-2}^{=}\lambda\frac{L}{2b\left(\varphi\right)}\frac{w^2}{2}\rho, \tag{2b}$$

$$\Delta p_{wyl}(\varphi) = \rho\left(1+\zeta_{wyl}\right)\frac{w^2}{2}. \tag{2c}$$

Regardless of the flow character in the clearance, the part of inlet drop in the whole pressure drop can be determined as:

$$\psi\left(\varphi\right) = \frac{\Delta p_{wl}}{\Delta p} = \frac{\zeta_{wl}}{\frac{\lambda L}{2b(\varphi)} + \zeta_{wl}}\ . \tag{3}$$

At the parallel axes and the eccentricity, the clearance width with the satisfying accuracy is determined by the formula [17, 3, 4]: $b \cong b_m + e\cos\varphi$, in which: $b_m = R_t - R_w$.

2.2 Laminar flow through the axial clearance

Designation of the pressure distribution in the axial clearance comes down to solve the Reynolds equation applied in the lubrication theory. The fluid flow in the clearance is forced by rotating shaft and axial pressure gradient. We assume the established axially-symmetrical flow of Newtonian fluid. Except the lower range of values, the system of motion equations (simplified one) can be accepted as [4, 10, 17] :

$$\frac{\partial^2 u}{\partial y^2} = 0, \quad \frac{\partial^2 v}{\partial y^2} = 0, \quad \frac{\partial p}{\partial z} = \mu\frac{\partial^2 w}{\partial y^2}. \tag{4}$$

Equation of continuity:

$$\frac{\partial u}{\partial x} + \frac{\partial v}{\partial y} + \frac{\partial w}{\partial z} = 0. \tag{5}$$

Boundary conditions for the coordinate system as in the Fig. 2:

$$y = b : u = v = c = 0,$$

$$y = 0 : u = u_0; v = 0; c = 0,$$

$$z = 0 : p = p_1,$$

$$z = L : p = 0$$

moreover:

$$u_0 = \omega r.$$

In the solution, one makes allowance for the influence of the pressure loss at the inlet to the clearance [3]:

$$p_{l1,2} = \frac{p_1}{b' - c' \cos\varphi},$$

$$b' = 1 + \frac{2b_m\left(\zeta_{wl}\right)}{\lambda L}, \tag{6}$$

$$c' = \frac{2e\left(\zeta_{wl}\right)}{\lambda L}. \tag{7}$$

From the equation of motion and equation of continuity, after substitution and transformation, we receive:

$$\frac{\partial^2 p}{\partial z^2} = \frac{12\mu}{b^3}\frac{u_0}{2}\frac{db}{dx}. \tag{8}$$

While integrating the above equation, taking into account the boundary conditions, we obtain the formula for pressure distribution in the axial clearance:

$$p\left(\varphi, z\right) = \frac{6\mu \sin\varphi}{\left(b_m + e\cos\varphi\right)^3}\frac{\omega e}{2}\left(Lz - z^2\right) + \frac{p_1}{b' - c'\cos\varphi}\left(1 - \frac{z}{L}\right). \tag{9}$$

2.3 Pressure drop in the clearance with turbulent flow, self-similar flow

Linear pressure drop along the clearance is determined by the Darcy-Weisbach formula (2b). It results from the assumption, that the resistance coefficient does not depend on the Reynolds number (self-similar flow called also auto-modelling).

While assuming the boundary conditions:

a) $p_1 = p\left(z = 0\right) = \left[1 - \psi\left(\varphi\right)\right]\Delta p$ – at the beginning of the clearance (behind the inlet),

b) $p_2 = p\left(z = L\right) = 0$ – overpressure value at the outlet of the clearance.

The pressure value at any point of the clearance is determined by the formula, [16]:

$$p\left(z, \varphi\right) = \left(1 - \psi\left(\varphi\right)\right)\Delta p\left(\frac{L - z}{L}\right). \tag{10}$$

In the above mentioned description, the influence of the peripheral speed inside the clearance wall is omitted.

2.4 Three-dimensional turbulent flow

For designation of flow structure, the commercial program CFX-TascFlow from AEA Technology Engineering Software company is used [1, 2].

The basic equations in the agreed system of Cartesian coordinates have the following form:

Equation of continuity:

$$\frac{\partial}{x_j}\left(\rho U_j\right) = 0 \tag{11}$$

where U_j represents Cartesian components of three-dimensional speed vector ($j = 1, 2, 3$);

- equation of momentum conservation:

$$\frac{\partial}{\partial t}(\rho\overline{U}_i) + \frac{\partial}{\partial x_j}(\rho\overline{U}_i\overline{U}_j) = -\frac{\partial\overline{p}}{\partial x_i} - \frac{\partial}{\partial x_j}\left\{\mu_{eff}\left(\frac{\partial\overline{U_i}}{\partial x_j} + \frac{\partial\overline{U_j}}{\partial x_i}\right)\right\} + f_i \tag{12}$$

where the term $f_i = -\rho\left(2\overline{\omega} \times \overrightarrow{\overline{U}} + \overline{\omega} \times (\overline{\omega} \times \overrightarrow{\overline{r}})\right)$ represents the Coriolis force

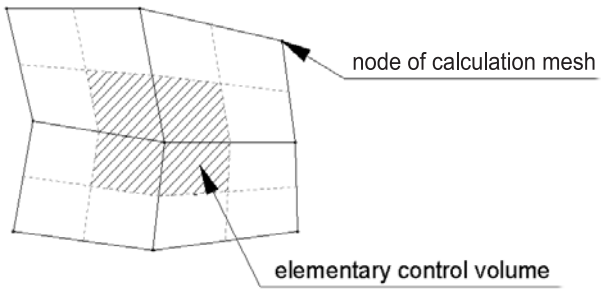

Figure 4. Placing the elementary control volume on the calculation mesh for integrating the basic equations.

and centrifugal force, in the system rotating with the angular speed $\overline{\Omega}$, where $\mu_{eff} = \mu + \mu_T$ and μ means the viscosity and μ_T turbulent viscosity determined from the selected model of turbulence.

The authors point out that the flow calculations in this type of clearances with the first-order digitisation gave the results significantly divergent from the results obtained in the experiments as well as while calculating with other methods. It is caused by appearing of the so called numerical viscosity in the first-order schemes [2, 8, 14].

The term value of Reynolds stresses apart from simple cases is unknown. The value of these stresses is related to averaging distribution of speed fields,

the relationship between the speed field and the stresses are closing equations. They are called the models of turbulence. In the calculations accomplished for this work, for determination of turbulent viscosity μ_T there are used the k-ε and two-layer model k-ε models of turbulence. Turbulent viscosity is proportional to the product of turbulent speed scale υ_t and Prandtl mixing path l_t, which was proposed by Prandtl and Kołmogorow.

$$\mu_T = \rho \cdot c_\mu \cdot \upsilon_t \cdot l_t \ . \tag{13}$$

In the model $k - \varepsilon$ the value υ_t is determined as the root from kinetic energy of turbulence $\upsilon_t = \sqrt{k}$. Whereas, the mixing path l_t l_t is connected with the equation, $\varepsilon = \frac{k^{\frac{3}{2}}}{l_t}$ where ε is an energy dissipation factor. After substitution, we obtain the relation on the dynamic turbulent viscosity $\mu_T = \rho \cdot c_\mu \frac{k^2}{\varepsilon}$, whereas k and ε are determined from the following differential equations:

– equation for k $\frac{\partial(\rho k)}{\partial t} + \frac{\partial(\rho U_j k)}{\partial x} = P_k - \rho\varepsilon + \frac{\partial}{\partial x_j}\left(\frac{\mu_T}{\sigma_k}\frac{\partial k}{\partial x_j}\right)$, (14)

– equation for ε $\frac{\partial(\rho\varepsilon)}{\partial t} + \frac{\partial(\rho U_j \varepsilon)}{\partial x} = \frac{\varepsilon}{k}(C_{\varepsilon 1} P_k - C_{\varepsilon 2}\rho\varepsilon) + \frac{\partial}{\partial x_j}\left(\frac{\mu_T}{\sigma_\varepsilon}\frac{\partial \varepsilon}{\partial x_j}\right)$ (15)

where $P_k = \mu_T \left(\frac{\partial U_i}{\partial x_j} + \frac{\partial U_j}{\partial x_i}\right)\frac{\partial U_i}{\partial x_j}$ is the turbulence energy production (16)

The constant models are as follows:

$$C_\mu = 0.09 \quad C_{\varepsilon 1} = 1.44 \quad C_{\varepsilon 2} = 1.92 \quad \sigma_k = 1.0 \quad \sigma_\varepsilon = 1.3$$

The above described, frequently used model of turbulence, in case of calculations for fluid-flow machine, requires using so called Wall Principle, in which the logarithmic speed distribution between the first node of calculation mesh lying in the flow area on the canal wall is assumed. In the flow model in the clearance under our examination, the value of Reynolds number can be within the range of laminar and intermediate flow. In this area, logarithmic speed distribution is not applied. Thereby, the two-layer model $k - \varepsilon$ is used, in which the flow area is separated into nodes where and nodes where $\frac{\mu_T}{\mu} < 36$. This separating criterion was proposed by Rodi [9]. In the external layer, the turbulent viscosity is determined from a two-equation standard $k - \varepsilon$ model [6]. In nodes, in which $\frac{\mu_T}{\mu} < 36$ the viscosity is determined by means of single-equation model. The value of dissipation energy ε is determined from the equation: $\varepsilon = \frac{k^{3/2}}{\ell_t f_\varepsilon}$. The turbulent viscosity is $\mu_T = \rho \cdot C_\mu \sqrt{k} \ell_t f_\mu$, where the mixing path: $\ell_t = \frac{\kappa \cdot y}{C_\mu^{3/4}}$,

$\kappa = 0.4$ – von Karman constant, y – node distance from the wall and in-flow functions: $f_\varepsilon = 1 - \exp\left(-\frac{y^+}{3.8 \cdot C_\mu^{1/4}}\right)$, $f_\mu = 1 - \exp\left(-\frac{y^+}{63 \cdot C_\mu^{1/4}}\right)$ in which y^+ is dimensionless node distance from the wall. The crucial issue is to control the values y+ during calculations.

In case of calculations with the standard k-ε model the value y+ should be included within the range 20-100, whereas for the two-layer model y+<2. In case of non-fulfillment of these conditions, the calculation mesh should be modified relatively.

In the calculations, the following boundary conditions are laid down:

1. value of total pressure in the greater pressure chamber,
2. value of static pressure in the smaller pressure chamber,
3. speed zeroing on the canal immovable walls,
4. values of peripheral speeds on the canal moveable walls,
5. turbulence intensity (at the level of 5%) and mixing path for the turbulence model $k - \varepsilon$ in the greater pressure chamber.

3 The force from pressure in the clearance and direction of its action

The components of the resultant radial force in the longitudinal eccentric clearance, acting on the shaft at the fluid flow can be calculated from the relation [12]:

$$F_y = \int_0^{2\pi} \int_0^L p(\varphi, z) \sin\varphi r d\varphi dz, \tag{17}$$

$$F_x = \int_0^{2\pi} \int_0^L p(\varphi, z) \cos\varphi r d\varphi dz. \tag{18}$$

The resultant force is:

$$F = \sqrt{F_x^2 + F_y^2}. \tag{19}$$

Angle of the resultant force action:

$$\varphi_F = \arctan\frac{F_x}{F_y}. \tag{20}$$

In the literature, the radial force formed from the pressure drop in the longitudinal eccentric clearance with immovable walls is called the Lomakin force. The

radial force formed in the longitudinal clearance with rotary walls however without the pressure drop between the inlet and outlet from the clearance is called the Bernoulli force. This force is characteristic for slide bearings.

4 Calculation example

Below there are compared the calculation results of pressure distribution in the clearance as well as of the radial force (Lomakin force) at the description as for: laminar flow, self-similar flow and model k-ε. The calculations are conducted at the set geometry of the clearance taking into account the pressure values at the inlet and outlet. The radii difference for one point in the clearance, resulting from the shift of impeller neck axle midpoints O_w and body bush O_t, is ignorably small. The fluid flowing through the clearance is water with temperature $t = 15°C$. In case of calculations done in TascFlow program and for the laminar flow, the rotational speed of rotary shaft amounted to $n = 0$ and $n = 2500$ rpm.
The clearance dimensions:

- clearance length $l = 111$ mm,
- shaft diameter $d_{wew} = 77.78$ mm $\pm$ 0.001 mm,
- bush diameter $d_{zew} = 80.11$ mm $\pm$ 0.01mm,
- relative eccentricity $\varepsilon = 0.85$.

Water flow parameter:

- inlet pressure $p_{wl} = 0.6$ MPa,
- outlet pressure $p_{wy} = 0.1$ MPa.

Reynolds criteria numbers [10]:

- in Poiseuille flow $\mathrm{Re}_P = \frac{2b_m c}{\nu} \approx 39000$, (21)
- in Couette flow $\mathrm{Re}_C = \frac{\omega r b_m}{\nu} \approx 0$ oraz 6136. (22)

5 Calculation results

The obtained pressure course is shown in the form of courses for the variable peripheral angles and clearance length in the whole range of data.

Calculations of pressure distribution (Figs. 5 and 6) done for laminar flow consider the inlet loss. In the self-similar flow, $\zeta_{wl} = 0.5$ is accepted and the outlet loss (i.e. $\zeta_{wyl} \approx 0$) is omitted. The omission of shaft rotation in the self-similar turbulent flow causes that the pressure courses (Fig. 7) are symmetrical towards

the forming one for the smallest and the greatest eccentric. The calculations conducted in TaskFlow program give the pressure distributions shown in Figs. 8 and 9. The net coordinates of the presented points are compliant with the net of points of measured pressure field (Figs. 10 and 11). The pressure measurement in the longitudinal ring clearance is conducted at 72 points with the holes with diameter 0.4 mm [15].

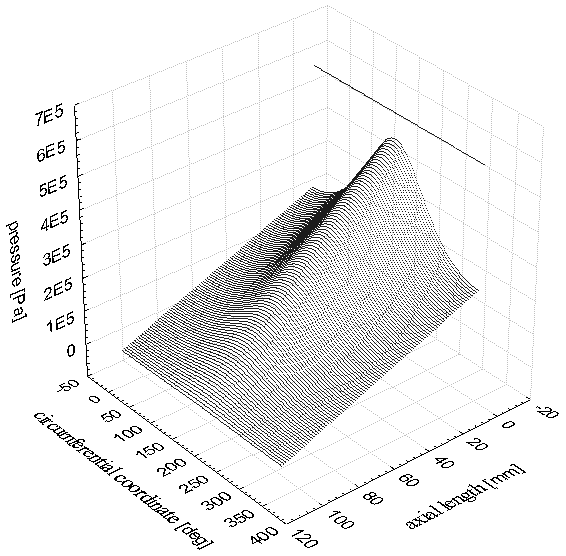

Figure 5. Calculated for the laminar flow of pressure field in the clearance at $n = 0$ rpm.

On the basis of obtained pressure fields, the values of Lomakin force are calculated (Fig. 12). Differences of the force values in the clearance, obtained from the numerical calculations and from calculated and measured pressure fields are significant. The decisive influence on the discrepancy of Lomakin force values has the different character of the pressure distribution along the clearance which appears behind the inlet section. In case of self-similar flow (Fig. 13), the scatter behind the inlet is decreased proportionally up to the outlet. For the measured pressure field (Fig. 14), the scatter of pressure values behind the inlet section undergoes a fast decrease.

The course of calculated pressure field is affected by the agreed values of the inlet loss factors and of linear loss factor. In the Figs. 15 and 16 the factor values, obtained from the measurement, are shown: of inlet loss and linear loss in the clearance with the variable relative eccentricity at the pressure drops $\Delta p = 0 \div 0.5$ MPa. The received values of the inlet loss factor for the axially-symmetrical clearance are smaller than usually agreed $\zeta_{wl} = 0.5$, which is confirmed in literature [17, 7]. The pressure increase at the outlet from the clearance is negligibly small.

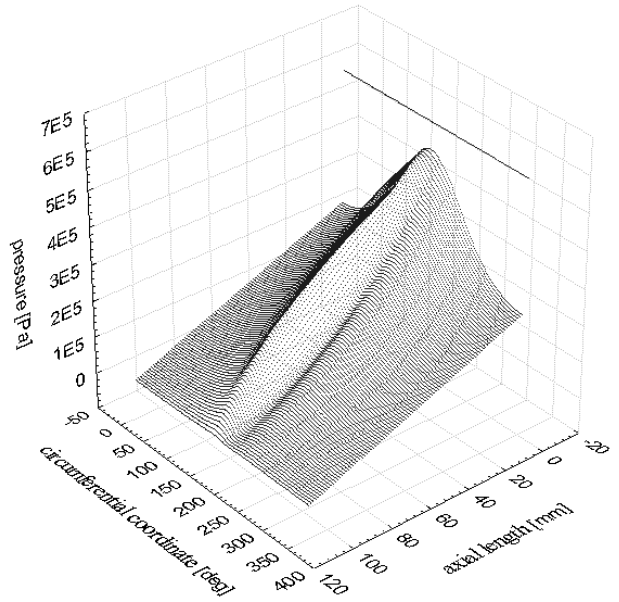

Figure 6. Calculated pressure field for laminar flow in the clearance at $n = 2500$ rpm.

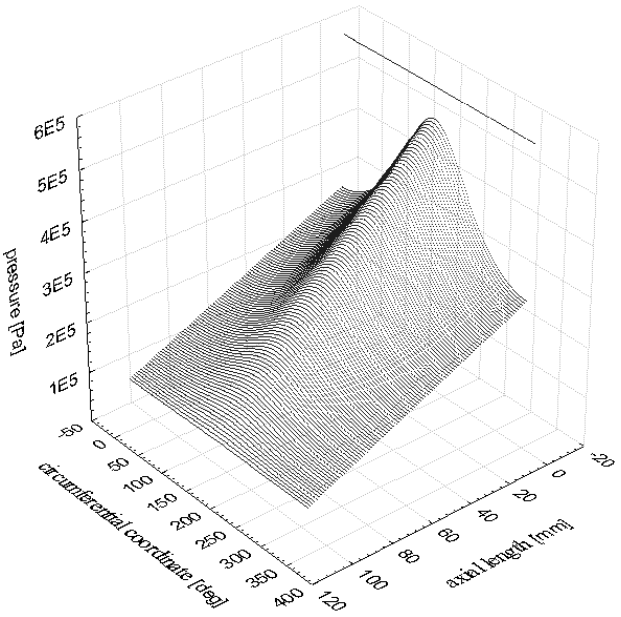

Figure 7. Calculated pressure field in the self-similar flow in the clearance at $n = 0$ rpm.

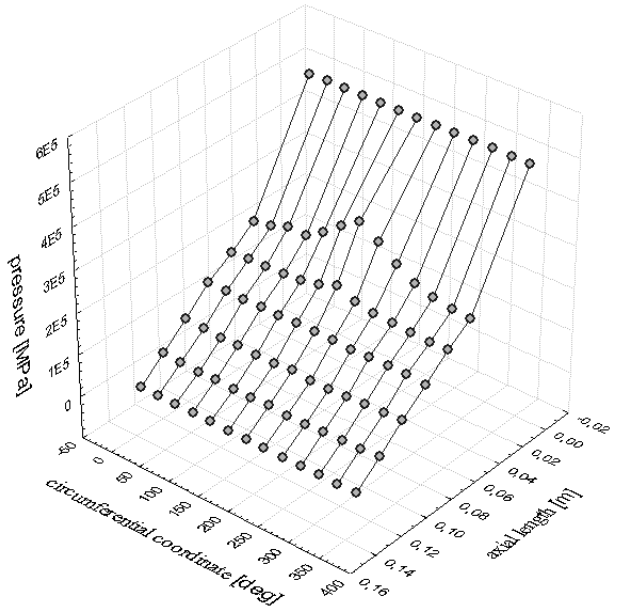

Figure 8. Calculated pressure field in the clearance in TascFlow program at $n = 0$ rpm.

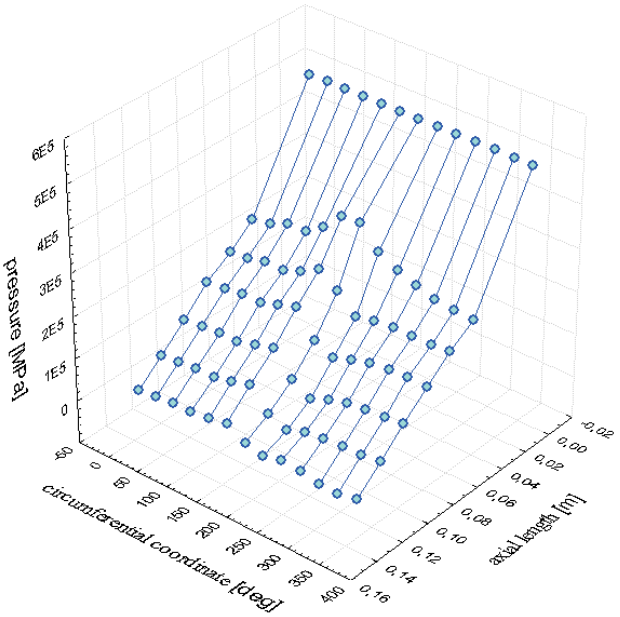

Figure 9. Calculated pressure field in the clearance in TascFlow program at $n = 2500$ rpm.

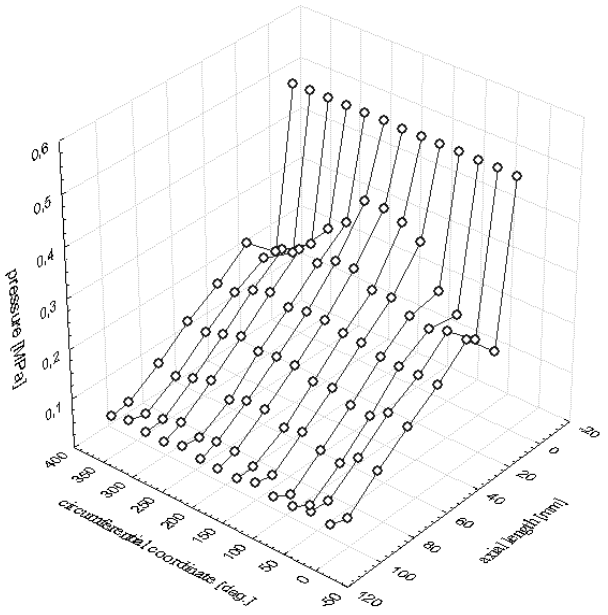

Figure 10. Measured pressure field in the clearance at $n = 0$ rpm.

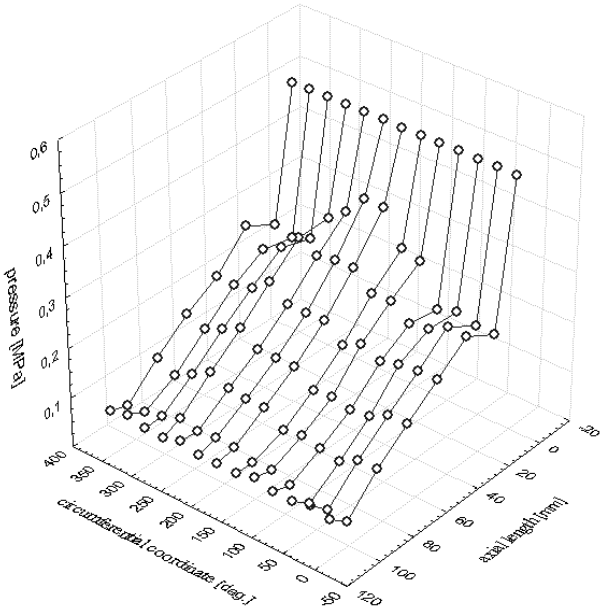

Figure 11. Measured pressure field in the clearance at $n = 2500$ rpm.

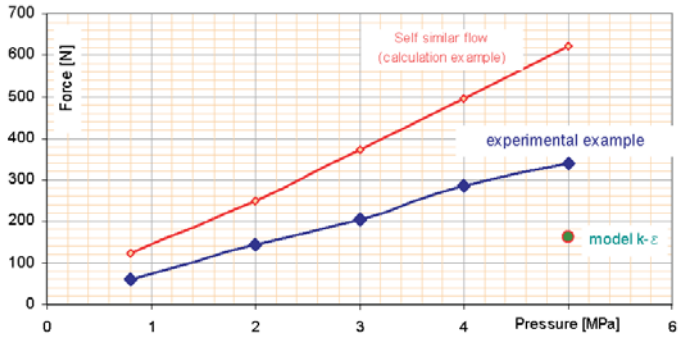

Figure 12. Comparison of Lomakin force values calculated on the basis of the measurement, calculated for the self-similar flow and with numerical method.

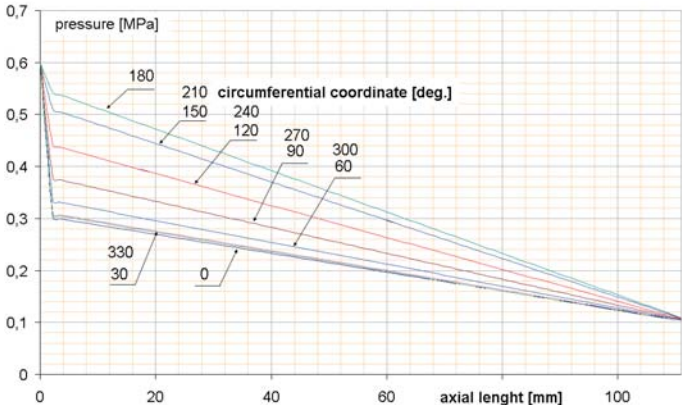

Figure 13. Calculated pressure distribution for the self-similar flow along the clearance.

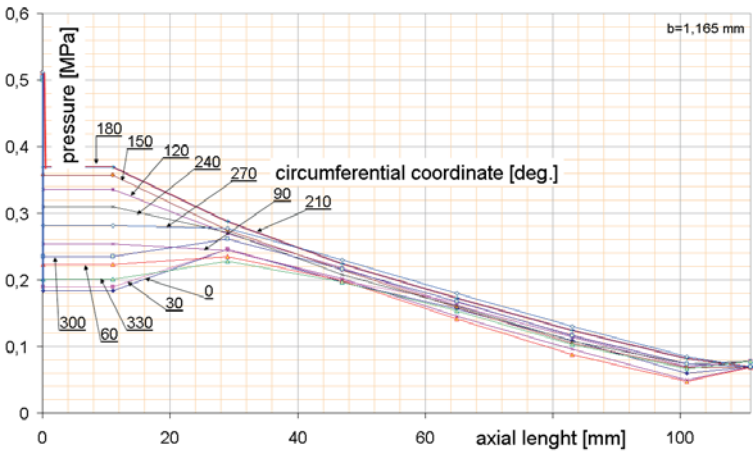

Figure 14. Measured pressure distribution along the clearance for $n = 0$ rpm.

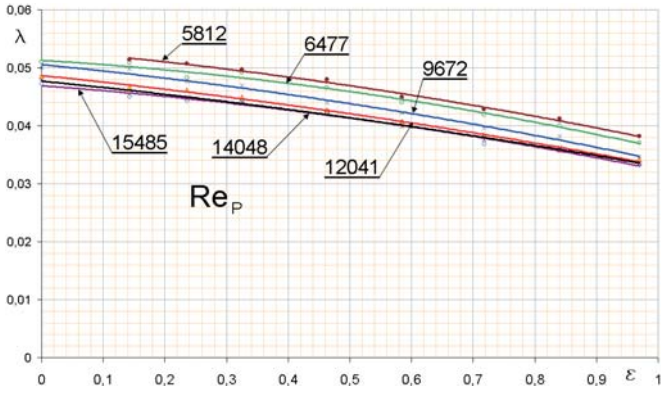

Figure 15. Linear loss factor in the eccentric function, $n = 0$ rpm.

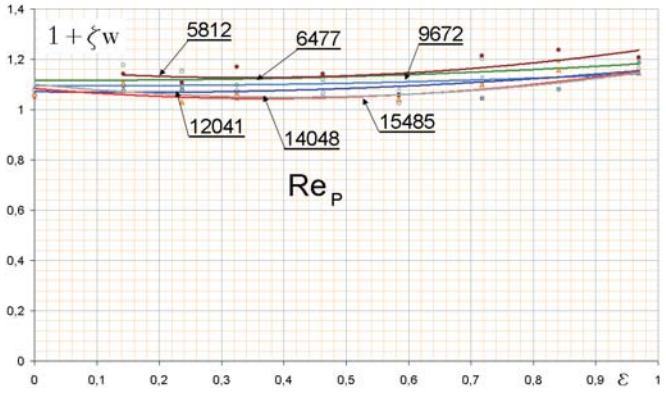

Figure 16. Inlet loss factor in the eccentric function $n = 0$ rpm.

6 Conclusions

The $k - \varepsilon$ model requires assuming of the value of k, which affects the calculation result significantly. The stream determination for the self-similar flow allows to verify the assumptions for the calculations with the model $k - \varepsilon$. The 'simplified' numerical calculations conducted for laminar and self-similar flow require assuming the values of inlet and continuous loss factors in the clearance. These values are well tested and shown in the literature for the longitudinal axially-symmetrical clearance, and more poorly and ambiguously for the longitudinal eccentric clearance.

The $k - \varepsilon$ model calculated Lomakin force in the longitudinal clearance is smaller than calculated for the turbulent and laminar flows than it resulted from the measurement. The increase of consistency of the results can be achieved by changing the factors of inlet loss $1 + \zeta_{wl}$ and linear loss λ along the clearance

perimeter. The exact value determination of Lomakin force in the longitudinal eccentric clearance requires further empirical testing.

Received 15 April 2008

References

[1] CFX-TASCflow Theory Documentation. Version 2.12. AEA Technology Engineering Software Limited Waterloo, Ontario, Canada N2L 5Z4.

[2] Chodkiewicz R., Papierski A.: *CFD Code a Useful Tool for the Turbomachinery Designer*, Seminar/Summer School CFD for Turbomachinery Aplications, 2001.

[3] Gryboś R.: *Fundamentals of Fluid Mechanics*, PWN, Warszawa 1989 (in Polish).

[4] Jędral W.: *Methods of Calculations of Longitudinal Forces and Relaxing Systems in Rotary Pumps*, Warsaw University of Technology Publishers, Warszawa 1988 (in Polish).

[5] Jędral W.: *Flows through Annular Clearences*, Mechanical Survey (Przegląd Mechaniczny), z. 11, 1979 (in Polish).

[6] Kazimierski Z.: *Numerical Determination of Turbulent Flows*, Ossolineum, Wrocław 1992 (in Polish).

[7] Korczak A. Papierski A.: *The flow through the face clearance of the disk relieving the axial force in multi-stage centrifugal pump*, Trans. of the IFFM, No. 115, 2004, 25-140.

[8] Papierski A., Rabiega M.: *Multiblock Paraller Computation of an Incompressible 3-D Flow in Turbomachines*, Task Quarterly 3, No. 1, 1999, 39-52.

[9] Rodi W.: *Experience with two-layer models combining the $k-\varepsilon$ model with a one-equation model near the wall*, American Institute of Aeronautics and Astronautics Paper 91-0216, American Institute of Aeronautics and Astronautics 29th Aerospace Sciences Meeting, Reno, Nevada, USA, January 7-10 1991.

[10] Tied W.: *Berechnung des laminaren uda turbulenten Reibungswiedestandes koncentrischer und exzentrischer Ringspalte*, Cemiker-Ztg./Chem Apparatur, 90 Jahrgang, nr 23. 1966.

[11] Troskolański A.T.: *Hydromechanics*, WNT, Warszawa 1962 (in Polish).

[12] Zarzycki M., G.Peczkis: *Optimisation of Inter-Overhaul Operation Period of Multistage Centrifugals Pumps*, TEMAG 2002, Ustroń (in Polish).

[13] Lomakin A.A.: *Razčet kritičeskogo čisla oborotov i uslovanija obezpečenija dinami/'eskoj ustojčivosti rotorov wysokonapornych gidravličeskich mašin s učetom cil, voznikajuščich b uplotenijach*, Energo-mašinostrojenije, No. 4, Moskva 1958.

[14] Marcinkovskij V.A., Karincev I.B.: *Vlijanije ščelevychuplotenij na kritičeske skorosti rotora pitatelnych nasosov*, Energomašinostrojenije, No. 4, Mockva 1961, 12-14.

[15] Marcinkovskij V.A.: *Vlijanije rotorov centrobežnych mašin*, Kniga 1, Sumy 2002.

[16] Čegurko L.E.: *Razgruzočnye ustrojstva pitatelnych nasosov teplovych elektrostancij*, Ènergija, Moskva 1978.

[17] Gryboś R.: *Dynamics of Rotating Machinery*, PWN, Warszawa 1994 (in Polish).

[18] Marcinkovskij V.A.: *Beskontaktnye uplotnienia rotornych mašin*, Mockva 1980, (publikacja wykonana w ramach Grantu KBN 8 T07B 006 21).

[19] Peczkis G.: *Analytical and Empirical Investigations of Pressure Distribution in Eccentric Longitudinal Clearence*, PhD Thesis, Gliwice 2007 (in Polish).